International Journal for Multidisciplinary Research (IJFMR)
E-ISSN: 2582-2160 ● Website: www.ijfmr.com ● Email: editor@ijfmr.com

Molecular Docking Method and Spectral Analysis and Electronic Structure Calculations on 4-Chlorobenzhydryl Chloride

M. Govindarajan

Department of Physics, Avvaiyar Government College for Women (AGCW), Karaikal, Puducherry 609 602, India, Arignar Anna Government Arts and Science College for Women (AAGASC),Karaikal Puducherry 609602, India

Abstract

In this work, the collective analyses of experimental and simulated fixed out by IR spectroscopy for 4-chlorobenzhydryl chloride (C13H10Cl2) (4CBENC) molecule in solid phase recorded. Density functional theory and Hartfock fundamental wavenumbers and intensity of the modes I fixed it with the aid of structure optimizations and normal force field computations based density functional theory (DFT) and ab-initio HF methods. The XRD data are closely related to optimized values. The complete assignments of wavenumbers were made on the basis of potential energy distribution (PED) of each vibrational mode. It will meet optimized geometries, which correspond to true energy minima, as revealed by the lack of imaginary frequencies in the vibrational mode calculation. Vibrational analysis at B3LYP/6-311++G(d,p) level, the thermodynamic functions were calculated and enthalpy changes (ΔH) slightly increased for the 4CBENC. The calculated HOMO and LUMO values for the molecules are also given with number of states 10. The electronic and excited state properties have been determined by TD-DFT method. The results of the calculations were applied to simulated spectra of the 4CBENC compound, which show good arrangements with observed spectra. The scaled B3LYP/6-311++G(d,p) results show the best results with the experimental values over the other methods. The energy, wavenumber and oscillator strength calculated by Time-Dependent Density Functional Theory (TD-DFT) complements with the experimental findings. The aim of RDG analysis is to look into non-covalent interactions in molecular and bring out their presence both internally and externally. In addition, molecular electrostatic potential (MEP) and electron density (ED) map of the 4CBENC were performed. The AIM analysis of the electronic structure of the 4CBENC molecule was carried out using a bond critical point (RC) and bond critical point (RB).

Keywords: FT-IR; FT-RAMAN; HOMO-LUMO; DFT/B3LYP and HF.

1. Introduction

The 4-chlorobenzhydryl chloride is fixed in Buclizine HCL, Meclizine HCL, Hydroxazine HCL The 4CBENC refractive index 1.60 and colorless to light yellow to light orange clear liquid Its specific gravity is 1.24. 4CBENC utilized in various scientific research applications such as, its derivatives synthesized from this compound are being studied for their potential use in cancer treatment due to their ability to inhibit cell proliferation and It is a clear, light yellow liquid that is slightly soluble in

chloroform, dichloromethane, and methanol. This compound is primarily used in the synthesis of various derivatives, particularly the pharmaceutical industry. It is mainly used in anticancer therapy drugs and clinically preferred to traditional treatment. This fact is avoiding resistance and toxicity drawbacks. These issues are preventing successful treatment and are responsible for cut survival times [1, 2]. It is used as an intermediate in the synthesis of benzhydrylpiperazine derivatives; it has shown cytotoxic properties against various cancer cell lines. These include anticancer, antifungal, antibacterial, antimalarial and antipsychotic agents [3-7], as well as HIV protease inhibitors and antidepressants [8-11]. The synthetic derivatives and natural products over the last 50 years have led to the discovery of the currently utilized anticancer drugs. It is used in the yield of fine chemicals and as a precursor in the synthesis of other complex compounds. These derivatives have been found to exhibit cytotoxic effects on cancer cells. The specific molecular and cellular effects of compounds are of ongoing research. It is known that the compound is sensitive to moisture, suggesting that environmental conditions such as humidity could potentially affect its stability and reactivity. It is known that it is used in the synthesis of derivatives. These derivatives have shown significant cell growth inhibitory activity on selected cancer cell lines. It is known to its effects at the molecular level through the synthesis of piperazine derivatives, which have cytotoxic effects. In industrial settings, the output of this compound may include the use of thionyl chloride as a chlorinating agent. This method advantageous due to its efficiency and the relatively high yield of the desired product

2. Experimental procedure

The molecule below investigating namely 4CBENC bought from Sigma-Aldrich chemicals, U.S.A with spectroscopic level and it was used as such without any further purification. The FT-IR spectrum of the compound has been recorded in Perkin-Elmer 180 Spectrometer in the range of 4000–400 cm^{-1}. The spectral resolution is ± 2 cm^{-1}. The FT-Raman spectrum of the compound was also recorded in the same instrument with FRA 106 Raman module equipped with Nd: YAG laser source operating in the region 100-4000 cm^{-1} at 1.064 μmline widths with 200 mW powers. The spectra were recorded scanning speed of 30 cm^{-1} min^{-1} and spectral width 2cm^{-1}. The frequencies of all sharp bands are accurate to ± 1 cm^{-1}.

3. Quantum chemical calculations

The entire quantum chemical calculations have been performed DFT (B3LYP) and ab-initio HF methods with 6-311++G(d,p) basis set using Gaussian 09 program [12]. The optimized structural parameters have been evaluated for the calculations of at different of theories. At the minimum geometry for the 4CBENC molecule no negative modes were obtained, therefore a true minimum on the potential energy of the molecule was found. As a result, the computed wavenumbers, reduced masses, force constants, infrared intensities, Raman activities, Raman intensities, and depolarization ratios were obtained. In order to improve the computed values in agreement with the experimental values, it is necessary to scale down the computed harmonic frequencies. Hence, the wavenumbers calculated at HF level are scaled by 0.905 [13] and the range of wave numbers above 1700 cm^{-1} are scaled as 0.958 and below 1700 cm^{-1} scaled as 0.983 for B3LYP/6-311++G(d,p) [14,15]. After scaled with the scaling factor, the deviation from the experiments is less than 10 cm^{-1} with a few exceptions. The appointments of the calculated normal modes have been made on the basis of the corresponding PEDs. The PEDs are calculated from quantum chemically computed wavenumbers using VEDA program [16]. Gauss view program [17, 18] has been considered to get visual animation and also for the verification of the normal modes

assignment.

The electronic absorption spectra for optimized 4CBENC calculated with time dependent density functional theory (TD-DFT) at B3LYP/6-311++G (d,p) level. To investigate the reactive sites of the title compound the molecular electrostatic potential was evaluated. Moreover, the changes in the thermodynamic functions (the heat capacity, entropy, and enthalpy) were investigated for the different temperatures from the wavenumbers calculations of title molecule.

4. Raman intensities

The Raman activities (S_{Ra}) calculated with Gaussian 09 program converted to relative Raman intensities (I_{Ra}) using the following relationship derived from the intensity theory of Raman scattering [30, 31]:

$$I_i = \frac{f\left(\nu_0 - \nu_i\right)^4 S_i}{\nu_i\left[1 - \exp\left(-hc\nu_i / kT\right)\right]}$$

where; ν_0 is the laser exciting wavenumber in cm^{-1} (in this work, we have used the excitation wavenumber $\nu_0 = 9398.5\ cm^{-1}$, which corresponds to the wavelength of 1064 nm of a Nd:YAG laser), ν_i the vibrational wavenumber of the i^{th} normal mode (cm^{-1}), while S_i is the Raman scattering activity of the normal mode ν_i. f (is a constant equal to 10^{-12}) is a suitably chosen common normalization factor for all peak intensities. *h, k, c* and *T* are Planck and Boltzmann constants, speed of light and temperature in Kelvin, respectively.

5. Results and discussion

5.1 Geometry analysis

The 4CBENC have two substituent group attached to form the molecule. The optimized DFT geometries by B3LYP/6-311++G(d,p) and molecular structure of the 4CBENC with atom numbering are shown in Fig.1. The internal coordinates describe the position of the atoms in terms of distances, angles and dihedral angles with respect to an origin atom. By allowing the relaxation of all parameters, the calculations are made up of scan coordinate1 C1-C2-C11-H12 and scan coordinate2 H12-C11-C13-C15 by rotating angle 0 to 360. It will meet optimized geometries, which correspond to true energy minima, as revealed by the lack of imaginary frequencies in the vibrational mode calculation. The symmetry coordinates are constructed using the set of internal coordinates. In this study, the full sets of 121 standard internal coordinates for 4CBENC are presented in Fig.2. This structure was found to be global minima on their potential energy surfaces, as the calculated vibrational spectra contain no imaginary wavenumber.

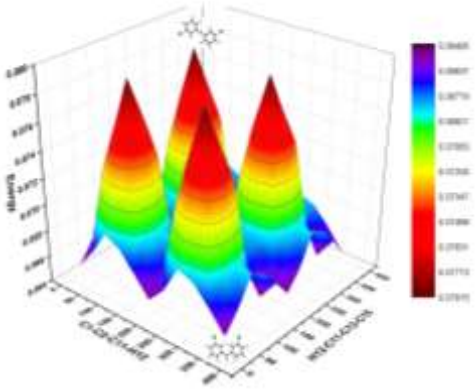

Fig 1

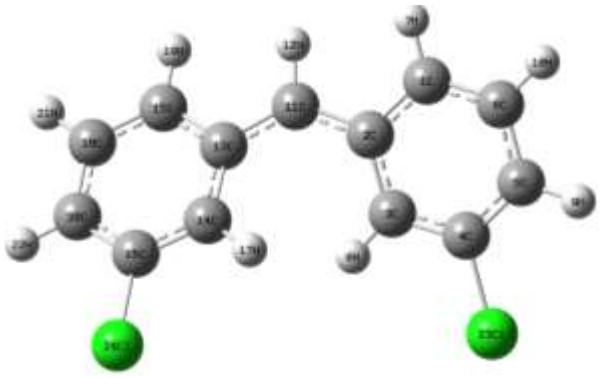

Fig 2

5.2 Thermodynamic Calculations

4CBENC thermodynamic parameters by DFT/B3LYP method 298.15 K and 1.00 atm pressure were fixed it in Table 1. The global minimum energy obtained for structure optimization of 4CBENC is. -1414.0083 a.u, and -1416.6516 a.u for B3LYP and HF methods with 6-311++G(d,p) basis sets. The mean difference in between the methods is ca. 4 a.u. only. All the above observations were made without any symmetric constrains. The rotational constants are falling in values from HF to B3LYP method. The thermal energies are also in the same trend with global minimum energy. I fixed it charge distribution of a molecule counts on the dipole moment in three dimensions and direction of the dipole moment in a 4CBENC show on the focus of positive and negative charges. The charged systems, its value depends on the selection of origin and molecular structure orientation.

Vibrational analysis at B3LYP/6-311++G(d, p) level, the thermodynamic functions: heat capacity (C) entropy (S) and enthalpy changes (ΔH) for the 4CBENC , I fixed it from the theoretic harmonic frequencies and listed in Table 1. From Table 1, it can be found that these thermodynamic functions with temperature ranging from 100 to 1000 K due to the fact that the molecular vibrational wavenumbers increase with temperature [19]. Correlation equations between heat capacities, entropies, enthalpy changes and temperatures I fixed it by quadratic polynomial formulas, and the corresponding fitting factors (R^2) for these thermodynamic properties are 0.999649, 0.99957 and 0.99809, respectively. The corresponding fitting equations are as follows and the correlation graph of those show in Figs. 3.

$C = -0.1185+0.1786T-7.4967x10^{-5}T^2$ ($R^2=0.99649$)

$S = 60.2247+0.1861T-3.7455x10^{-5}T^2$ ($R^2=0.99957$)

$\Delta H = -1.7960+0.0292T+4.1637\ 10^{-5}T^2$ ($R^2=0.99809$)

The thermodynamic data furnish helpful information for the further study of the 4CBENC. I fixed it to compute the early thermodynamic energies according to relationships of thermodynamic functions and calculate directions of chemical reactions according to the second law of thermodynamics in thermo chemical field [20]. Notice: all thermodynamic computations were acted in gas phase and they could not be used in solution.

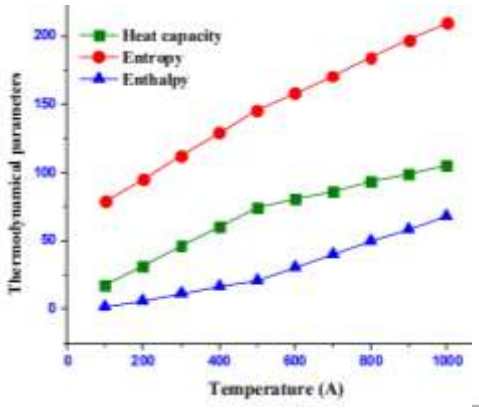

Fig 3

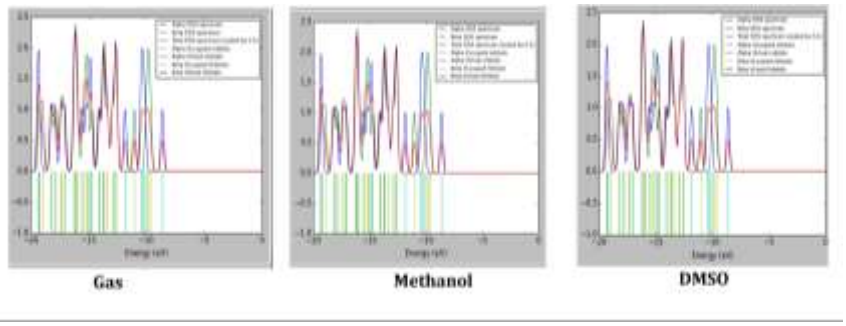

Fig 4

5.3 Ultraviolet spectra and Frontier molecular orbital (FMO) analysis

The highest occupied molecular orbitals (HOMOs) and the lowest-lying unoccupied molecular orbitals (LUMOs) are named as frontier molecular orbitals (FMOs). The FMOs play a key role in the optical and electrical properties, as well as in UV–Vis spectra [21]. Gauss-Sum 2.2 Program [22] was used to calculate group contributions to the molecular orbital (HOMO and LUMO) and prepare the density of the state (DOS) as shown in Fig.4 and 5. The HOMO is the power to give an electron, LUMO as represents the ability to obtain an electron. The gap between HOMO and LUMO energy determines the kinetic stability, chemical responsiveness and, optical polarization and chemical hardness–softness of a 4CBENC.

In order to measure the energetic behavior of a 4CBENC compound, we carried out calculations in Gas, Methanol, and DMSO with number of states 10. According to the probe of FMO energy levels of a 4CBENC, we can find that the corresponding electronic shift encountered between HOMO and LUMO, HOMO-1 and LUMO+1, respectively. The energies of four important molecular orbital of a 4CBENC the highest occupied MO's (HOMO and HOMO−1), the lowest and the second lowest unoccupied MO's (LUMO and LUMO+1) I fixed it using B3LYP/6-311++G(d,p). The calculated energy values of HOMO and HOMO-1 are -8.5793 and -10.1129 eV Gas, respectively. LUMO and LUMO+1 is 3.2758 and 3.5334 eV in the same respectively. The value of energy gap between the HOMO and LUMO is -5.3034 eV in Gas, respectively.

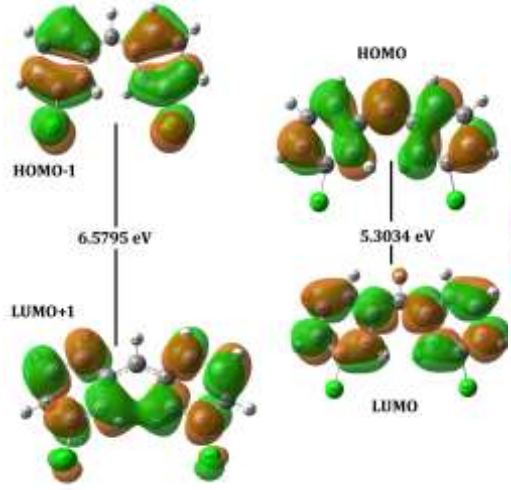

Fig 5

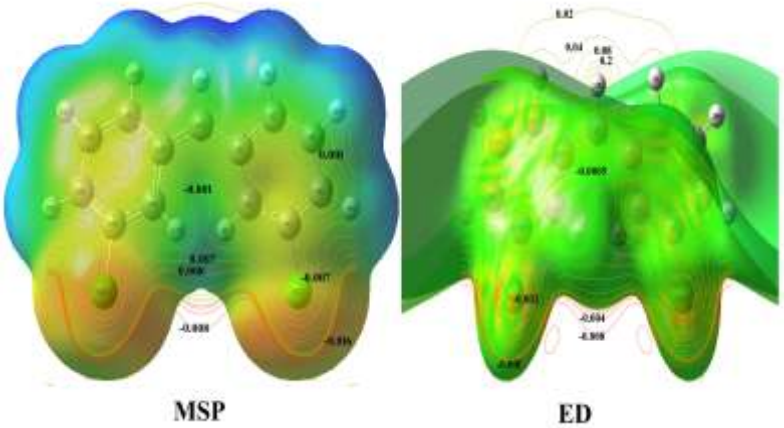

Fig 6

The calculated HOMO and LUMO moment values for the molecules are also given for Gas, Methanol, and DMSO in the Table 2. An ultraviolet spectra analysis of 4CBENC has been investigated in Gas, Methanol and DMSO by theoretical calculation. On the basis of fully optimized ground-state structure, TD-DFT/B3LYP/6-311++G(d, p) calculations were fixed it to determine the low-lying excited states of 4CBENC. The theoretical electronic excitation energies, oscillator strengths and absorption wavelength are fixed it in Table 5. Calculations of the molecular orbital geometry show that the absorption maximums of this molecule correspond to the electron transition between frontier orbitals such as translation from HOMO to LUMO. As can be seen in Table 5, the calculated absorption maxima values have been found to be 272.75, 252.55, 251.91, 237.83 and 220.49 nm for gas, 260.294, 253.757, 218.707, 214.481, 213.827, 207.743, 207.666, 204.832, 204.724 and 194.934 nm for gas at DFT/B3LYP/6-311++G(d,p) method. It is seen from Table 2, calculations performed at gas are close to each other when compared with other phases.

5.4 Optimized structure molecular and electrostatic potential

In the present study, a 3D plot of molecular electrostatic potential (MEP) and electron density (ED) map of 4CBENC I fixed it in Fig. 6. The MEP that is a plot of electrostatic potential mapped onto the constant electron density surface. The MEP is a useful property to study reactivity given that an approaching electrophile to negative regions (where the electron distribution effect is dominant). In the majority of the MEPs, while the maximum negative region, which preferred site for electrophilic attack indications as red colour, the maximum positive region which preferred site for nucleophilic attack symptoms as blue colour. The negative electrostatic potential I fixed it to nitrogen preoccupied region and $(CH_2)_2$ the positive electrostatic potential corresponds to the repulsion of the proton by atomic nuclei in regions where low electron density exists and the nuclear charge I fixed it (and shades of blue of colour). The importance of MEP lies in the fact that it collectedly exhibits molecular shape as well as positive, negative and neutral electrostatic potential regions in terms of colour grading (Fig. 7) and is very useful in research of molecular structure with its physiochemical property relationship [23-25].

I fixed it different values of the electrostatic potential at the surface are represented by different colors. Potential increases in the order red < orange < yellow < green < blue. The color code of this map is in the range of -0.05929 a.u. (deepest red) to 0.05929 a.u. in compound. Where blue indicates the strongest attraction and red indicates the strongest repulsion. The ED value of the 4CBENC is found to be within the range -0.01766 to +0.01766 a.u. The regions having the positive potential are over all hydrogen atoms. I fixed it front and side view of carbon in 4CBENC is having green colour, and it shows neutral potential. According to these calculated results, the MEP map shows that the negative potential sites are on carbon and chlorine atoms as well as the positive potential sites are around hydrogen atoms.

5.5 Mode analysis

The maximum number of potentially observable fundamentals of a non-linear molecule, which contains N atoms is equal to (3N-6), apart from three translational and three rotational degrees of freedom [26, 27]. Hence, 4CBENC molecule, that was planar, has 24 atoms with 66 normal modes of vibrations and considered under C_s point group symmetry. The fundamental modes are distributed in the C_s symmetry species as: $\Gamma_{vib} = 45A' + 21A''$. Here, A′ is symmetric planer and A″ asymmetric non-planer vibrations. All vibrations are active both in Raman and infrared absorption. The detailed vibrational assignments of the experimental wavenumbers are I fixed it normal mode analyses, and a comparison with theoretically

scaled wavenumbers with PED by B3LYP methods. Since the scaled wavenumbers following B3LYP/6-311++G(d,p) method are fixed it closest to experimental data than the results obtained using other methods. The observed and simulated FT-IR spectra of 4CBENC are shown in Fig. 7, respectively. The observed and scaled theoretical frequencies using HF/6-311++G(d,p) and DFT/B3LYP/6-311++G(d,p) basis set with PEDs I fixed it in the Table 3.

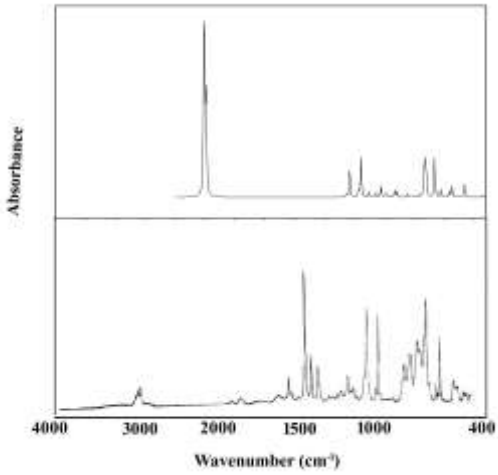

Fig 7

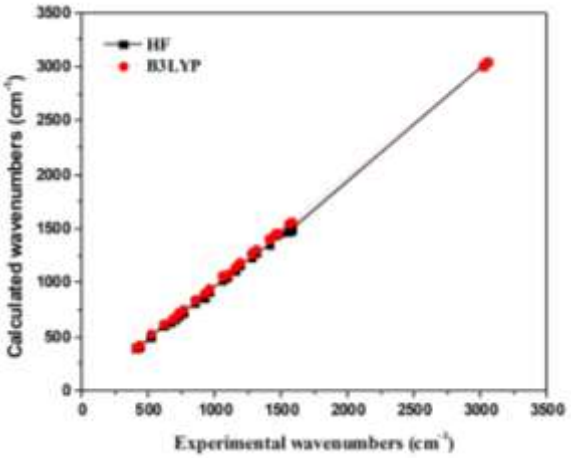

Fig 8

5.5.1 C-H vibrations

The aromatic derivatives are give rise to C-H stretching, C-H in-plane and C-H out-of-plane bending vibrations. Aromatic compounds commonly exhibit multiple weak bands in the region 3100–3000 cm^{-1} [28] due to aromatic C-H stretching vibrations. In pure naphthalene I fixed it in the region 3080–3000 cm^{-1}. They are not appreciably affected by the nature of the substituent [29-31]. All the C–H stretching vibrations are very weak in intensity in the 4CBENC. Here, the C–H vibrations of the title compound are observed at 30820 and 3020 cm^{-1} in FT-IR spectrum with very weak intensities. This mode I fixed it in the range 3038-2993 cm^{-1} with B3LYP/6-311++G(d,p).

The bands due to C-H in-plane bending vibrations I fixed it in the region 1000–1300 cm^{-1} [32]. For this compound, the C-H in-plane bending vibrations were observed at 1190, 1175, 1150, 1095 and 1055 cm^{-1} in FT-IR. The theoretically scaled vibrations by B3LYP/6-311++G (d,p) level method also shows good agreement with experimentally recorded data.

The C-H out-of-plane bending vibrations I fixed it in the region 980-717 cm^{-1} in [32]. The vibrations are identified at 760, 720, 695, 668 and 610 cm^{-1} in FT-IR are assigned to C-H out-of-plane bending for 4CBENC. All vibrations I fixed it as pure mode except first one from PED values. The C-H out-of-plane bending vibrations are also lie in the characteristic region

5.5.2 Ring vibrations

The aromatic ring modes I fixed it more C-C bands. The ring stretching vibrations I fixed it in the region 1300-1000 cm^{-1} [33, 34]. Most of the ring modes I fixed it by the substitution of aromatic ring. In present study, the bands with are of different intensities and I fixed it at 1575,1550, 1475, 1450, 1410, 1310 and 1275 cm^{-1} in FT-IR have been assigned to C-C stretching vibrations. The theoretically calculated values at 1569-1254 cm^{-1} by B3LYP/6-311++G(d,p) method. It shows the theoretic values excellent agreement with experimental data. All these vibrations I fixed it with mixed modes in PED

except their and evident by its strong intensity. As expected, the in-plane deformations I fixed it at higher frequencies than the out-of-plane vibrations.

5.5.3 C-Cl vibrations

The mixing of vibrations are possible due to the lowering of molecular symmetry and the presence of heavy atoms [35-38]. According to these early reports, the C–Cl stretching band I fixed it around 505–380 cm^{-1}. In FT-Raman spectrum of 4CBENC, a strong band at 405 cm^{-1} I fixed it to C-Cl stretch vibration. The theoretical wavenumber of C-Cl stretching vibration 403 cm^{-1} by B3LYP/6-311++G(d,p) coincides very well with the experimental value. The C-Cl in-plane bending and out-of-plane bending vibrations are expected to the bands, respectively. The mean difference between experimental and calculated (B3LYP/6-311++G(d, p)) values of C-Cl vibrations is only 3 cm^{-1}. The computed values for C–Cl in-plane and out-of-plane bending vibrations by B3LYP/6-311++G(d,p) method nearly coincides with experimental values.

5.6 Error analysis in B3LYP and HF calculations

The standard deviation is very small in B3LYP/6-311++G(d,p) method. The unscaled theoretical wavenumbers, I fixed it and scaled by different scaling factors. This event is quite obvious, since calculated frequencies are harmonic in nature, whereas experimental frequencies may include anharmonicity. In order to reduce the standard deviation between the unscaled and observed fundamentals, scale factors I fixed it. The theoretical values in different methods are in harmonic nature. A close agreement between the experimental and scaled wavenumbers is mostly achieved in the fingerprint region. It is proved by Fig. 8 drawn between experimental frequencies and error with calculated frequencies. HF and DFT (B3LYP) methods I fixed it a uniform deviation after scaling. In this, the HF methods showed more deviation than the DFT methods. The relation is usually linear and described by the following equation (x-experimental frequency):

B3LYP

$$\partial cal = 1.2 + 1\ \partial exp \qquad (R^2 = 0.99919)$$

HF

$$\partial cal = -30.24 + 1\ \partial exp \qquad (R^2 = 0.99989)$$

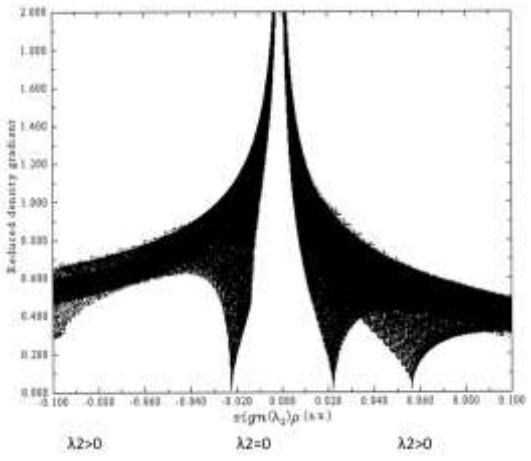

Fig 9

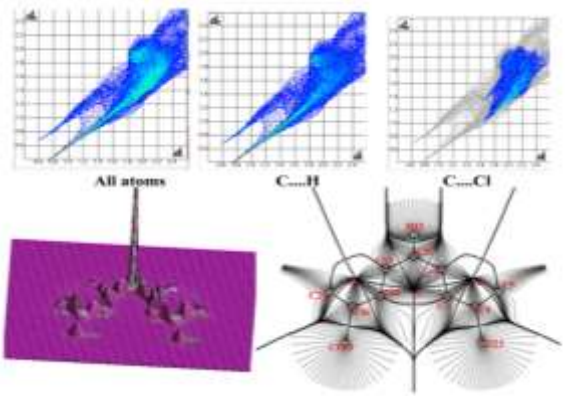

Fig 10

It clearly indicates, the calculated frequencies by B3LYP/6-311++G(d,p) method is exactly fit with experimental frequencies.

5.7 Analysis of molecule Reduced density gradient (RDG)

The aim of RDG analysis is to look into non-covalent interactions within molecular and bring out their presence both internally and externally. The Fig.9 shows the RDG plot of the molecule in question. The RDG grid is drawn between RDG and [(λ_2) ρ] a.u. Here, the symbol (λ_2) ρ is the second eigenvalue of the electron density. In the figure, the value of the symbol (λ_2) ρ > 0 represents a negative interaction, while the value of the symbol (λ_2) ρ < 0 represents a positive interaction. The symbol (λ_2) ρ =0 is the weak van der Waals interaction and λ_2 has a range from -0.050 to 0.020. RDG plot shows a positive peak identifying insufficiency in the benzene ring [39]. The positive peaks are between 0.020 and 0.100. I fixed it spikes in the picture represent the attraction of hydrogen atoms. The blue line occurs between -0.050 and -0.100. Weak interactions I fixed it in the 0.040 to 0.020. Thus, RDG elements confirm the interaction site in the molecular structure of the compound.

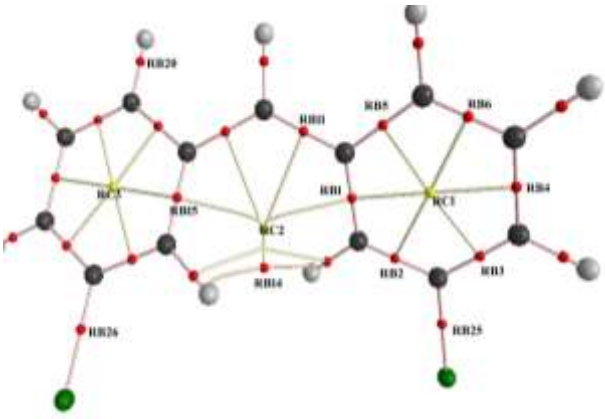

Fig 11

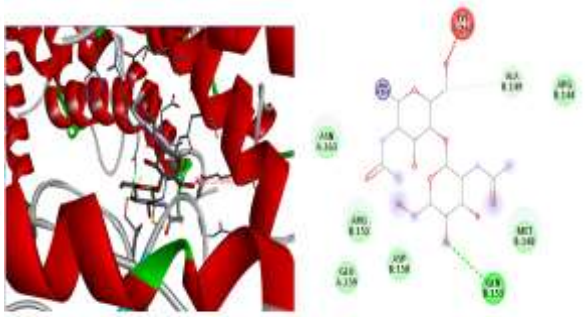

Fig 12

5.8 Topological analysis of molecule

The AIM analysis of the electronic structure of the 4CBENC molecule I fixed it out using a bond critical point (RC) and bond critical point (RB) as shown in the Table .4 [40]. The CP search for all bonds invariably finds a (3,-1) bond critical point (RB). The negative Laplacian of electron density shows the covalent bond character of bonds in the molecule. I fixed it the critical point is the point where the first derivative of electron density. The electron density BCP is a physically observable quantity, which is near the nucleus and appears to be featureless elsewhere [41]. I fixed it to analyze the bonding situation and chemical reactivity [42], whereas the Laplacian of electron density r2 BCP(r) of the bond measures the extent of depletion or concentration of charges. The position of the BCP gives an idea of the polarity of the bond. The static deformation density maps of theory Fig. 10 and 11, display the electron density associated with the lone pairs of oxygen Cl and nitrogen (C16 and C4) atoms in the molecule. I fixed it BCP positions are moved towards the H, BCP position is 28.9% away from the bond midpoint atom range from H atom. A bond-path analysis I fixed it to determine the polarization of the bonds. All the bonds are polarized, and their BCP positions are moved towards the C atom. The Laplacian of the electron density analysis gives information about the chemical features of the molecule. If the atoms of a chemical bond have a shared interaction then its Laplacian is r2 BCP(r) < 0 and if r2 BCP(r) > 0. Then the interaction is a closed-shell interaction. The BCP(r) value of C-C bonds of the 4CBENC at the BCP

varies from C20, C14, C1, C5, C3 and Cl24 are fixed it the Fig 11. The Laplacian of the C-Cl bond is the important role of the bond.

5.9 Molecular docking of molecule

The molecular docking is estimated forecasts small or macromolecules' molecular interactions and binding patterns in contact with a receptor. This theory is explaining, molecular recognition happens when a receptor protein's binding site, like a key in a lock, precisely matches the structure of a ligand. The Schrödinger software, molecular docking studies were carried out for the chemical to determine the potential target. In the present work, rigid receptor docking I fixed it, and the highest accuracy glide score (XP Score) I fixed it to assess the best molecular docked complexes. The XP is a measure of ligand binding energy derived from applying force field components and docking results, which importantly influence the interaction amongst the ligand and the receptor. To obtain these values, the three-dimensional (3D) structures of the target proteins (ASN A: 263, ARG B: 151, ASP B: 150, GLU A: 259, GLN B: 153, MET B: 148 and ALA B: 149) I fixed it from the Protein Data Bank (PDB) [53]. The three energetic binding sites of each protein I fixed it as 5.19, 5.9 and 6.0 within a cubic with grid points with binding efficiency 0.35, 0.39 and 4.0. The Fig.12 shows the compound's best lock and 2D diagram of with its target protein. The molecule is more likely to bind to its target protein when the optimized conformation I fixed it.

5.10 Characterization of Ramachandran plot of molecule

The calculated ϕ and ψ are between +180° and –180°,(i.e. 360° of rotation for each). They are possible in reality due to the physical encounters of atoms in 3-dimensional lattice. These physical lattices fix steric interference. The values of ϕ and ψ I fixed it due to steric interference between non-bonded atoms. The polypeptide shapes are defined by the values of ϕ and ψ. Most values of ϕ and ψ are not allowed due to steric interference between non-bonded atoms. In the Fig 13, shows the Ramachandran plot. The parts I fixed it for all amino acids except glycine, which is unique as it lacks a side chain. The dark blue regions called allowed regions correspond to conformations where there are no steric interferences. Most of ϕ and ψ values of a polypeptide chain fall within these allowed regions of the Ramachandran plot. Antiparallel β-sheet, ϕ and ψ are lie in the region -50 to -150 and 100 to 170. Corresponding, Parallel β-sheet ϕ and ψ are lie in the region -75 to -135 and 70 to 135. The left-handed and right-handled α-helix I fixed it in the Table .5. Light blue regions correspond to conformation having the outer limit van der Waals distances i.e. the atoms are allowed to come a little closer together

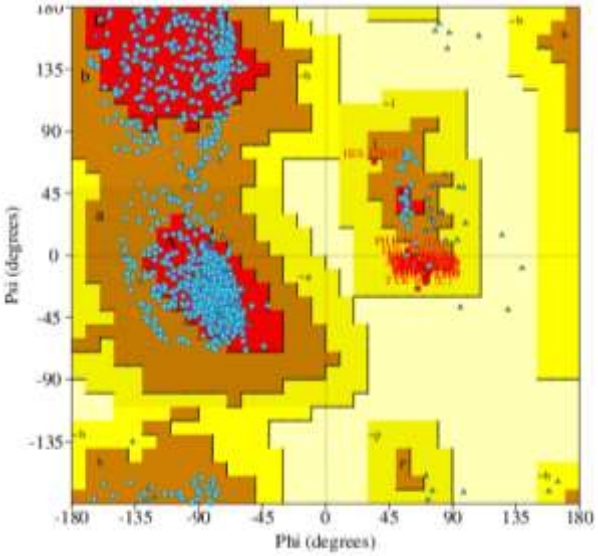

Fig 13

6. Conclusion

The infrared vibration I fixed it and assigned to 4CBENC molecular crystal. The normal co-ordinate of molecule I fixed it DFT-B3LYP method with 6-311++G(d, p) basis set and HF method with 6-311++G(d, p) basis sets. The estimated bond angle values suggest that the ring of the molecule I fixed it due to the steric and electronic effects. The correlation equations between heat capacities, entropies, enthalpy changes and temperatures are fixed it by quadratic polynomial formulas. The energy break of HOMO–LUMO explains the charge shift interaction in a 4CBENC, which influences the physiologic and biological activity of the molecule. The HOMO→LUMO passage involves an electron density transfer from chlorine atom. The calculations are executed when Gas, Methanol, and DMSO are near to each other. The maps are in the range between -0.05929 a.u. (deepest red) to 0.05929 a.u. in 4CBENC. The mean difference between experimental and calculated (B3LYP/6-311++G(d,p)) values of C-Cl vibrations is only 3 cm^{-1}. The vibrations of C-C I fixed it with mixed modes in PED except three and evident by its strong intensity. The C–H vibrations of the title compound are observed in FT-IR spectrum with very weak intensities. The calculated frequencies by B3LYP/6-311++G(d,p) I fixed it with experimental wavenumbers. The RDG elements confirm the interaction site in the molecular structure of the compound. The symbol is the weak van der Waals interaction and λ2 has a range from -0.050 to 0.020. The Laplacian of the C-Cl bond is the important role of the bond. The three energetic binding site of each protein are enclosed as 5.19, 5.9 and 6.0. I fixed it parallel β-sheet ϕ and ψ are lying in the region -75 to -135 and 70 to 135. The molecule is more likely to bind to its target protein when the optimized conformation is fixed it.

References

1. Mencher.S.K, Wang.L.G, Promiscuous drugs compared to selective drugs (promiscuity can be a virtue). BMC Clin. Pharmacol. 2005, 5, 3–7.
2. Jimeno.A, Hidalgo.M, Multitargeted therapy: Can promiscuity be praised in an era of political correctness. Crit. Rev. Oncol. Hematol. 2006, 59, 150–158
3. Hulme.C.Ma.L, Romano.J, Morisette.M, Novel applications of ethyl glyoxalate with the Ugi MCR. Tetrahedron Lett. 1999, 40, 5295–5299.

4. Gabriel.F.E, Gu.J, Slater.L.M, Hara.K, Jacobs.J.W .Tumor apoptosis induced by epoxide-containing piperazines, a new class of anti-cancer agents. Cancer Chemother. Pharmacol. 2000, 45, 183–191.
5. Gillet.R, Jeannesson.P, Sefraoui.H, Arnould-GueArin.M, Kirkiacharian.L.S, Jardillier.J.C, Pieri.F. Piperazine derivatives of butyric acid as differentiating agents in human leukemic cells. Cancer Chemother. Pharmaco. 1998, 41, 252–255.
6. Upadhayaya.R.S, Sinha.N, Jain.S, Kishore.N, Chandra.R, Arora.S.K. Optically active antifungal azoles: Synthesis and antifungal activity of (2R,3S)-2-(2,4-difluorophenyl)-3-(5-[2-[4aryl-piperazin-1-yl]-ethyl]-tetrazol-2-yl/1-yl)-1-[1,2,4]-triazol-1-yl-butan-2-ol. Bioorg. Med. Chem. 2004, 12, 2225–2238.
7. Choudhary.P, Kumar.R, Verma.K, Synthesis and antimicrobial activity of N-alkyl and N-aryl piperazine derivatives. Bioorg. Med. Chem. 2006, 14, 1819–1826.
8. Askin.D, Eng.K.K, Rossen.K, Purick.R.M, Wells.K.M, Volante.R.P, Reider.p.J, Highly diasteroselective reaction of a chiral, non-racemic amide enolate with (S)-glycidyl tosylate. synthesis of the orally active HIV-1 protease inhibitor L-735,524. Tetrahedron Lett. 1994, 35, 673–676.
9. Dorsey.B.D, Levin.R.B, McDaniel.S.L, Vacca.J.P, Guare.J.P, Darke.P.L, Zugay.J.A, Emini.E.A, Schleif.W.A, The design of a potent and orally bioavailable HIV protease inhibitor. J. Med. Chem. 1994, 37, 3443–3451.
10. Rosen.K, Weissman.S.A, Sager.J, Reamer.R.A, Askin.D, Volante.R.P, Reider.P.J . Asymmetric Hydrogenation of tetrahydropyrazines: Synthesis of (S)-piperazine 2-tert-butylcarboxamide, an intermediate in the preparation of the HIV protease inhibitor indinavir. Tetrahedron Lett. 1995, 36, 6419–6422.
11. EGYT. Pyridine Derivatives Having Antidepressant Activity. U.S. Patent 3,865,828, 11 February 1975.
12. Frisch.M.J. et al, Gaussion 09 Program, Gaussian, Inc., Wallingford, CT, 2004.
13. Young.D.C, Computational Chemistry: A Practical Guide for Applying Techniques to Real World Problems (Electronic), John Wiley & Sons Inc., New York, 2001.
14. Karabacak.M, Coruh.A, Kurt.M, J. Mol.Struct. 892 (2008) 125-131.
15. Sundaraganesan.N, Illakiamani.S, Saleem.H, Wojciechowski.P,M, Michalska.D, Spectrochim. Acta 61A (2005) 2995.
16. Jamróz.M.H, Vibrational Energy Distribution Analysis, VEDA 4, Warsaw, 2004.
17. Frisch.A, Nielsen.A.B, Holder.A.J., Gaussview Users Manual, Gaussian Inc., Pittsburg.
18. Dennington.R.I, Keith.T, Millam.J, Eppinnett.K, W.Hovell, Gauss View Version 3.09, 2003.
19. H.K.Fun, C.K.Quah, M.I.Attia, M.S.Almutairi, Ghoneim.S.W, Acta Cryst. E68, (2012) 27
20. BevanOtt.J, Boerio-Goates.J, Calculations from Statistical Thermodynamics, Academic Press, 2000.
21. Zhang.R, Dub.B, Sun.G, Sun.Y, Spectrochim. Acta A 75 (2010) 1115–1124.
22. Fleming.I, Frontier Orbitals and Organic Chemical Reactions, Wiley, London, 1976.
23. Murray.J.S, Sen.K, Molecular Electrostatic Potentials, Concepts and 399 Applications, Elsevier, Amsterdam, 1996.
24. Scrocco.E, Tomasi.J, in: P.Lowdin (Ed.), Advances in Quantum Chemistry, Academic Press, New York, 1978.
25. Sponer.J, Hobza.P, Int. J. Quant. Chem. 57 (1996) 959.

26. Silverstein.R.M, Bassler.G.C and Morrill.T.C, Spectrometric identification of organic compounds, John Wiley, Chichester, 1991.
27. Socrates.G, Infrared and Raman Characteristic Group Frequencies–Tables and Charts.third ed., Wiley, New York, 2001.
28. Krishnakumar.V, Xavier.R.J, Indian J.Pure Appl. Phys., 41 (2003) 597.
29. Colthup.N.B, Daly.L.H, Wiberley.S.E, Introduction to Infrared and Raman Spectroscopy, Academic Press, New York, 1990.
30. Dollish. F.R, Fateley.W.G, Bentley.F.F, Characteristic Raman Frequencies of Organic Compounds, Wiley, New York, 1997.
31. Varsanyi.G, Vibrational Spectra of Benzene Derivatives, Academic Press, New York, 1969.
32. Srivastava.A, Singh.V.B, Indian J. Pure. Appl. Phys 45 (2007) 714-720.
33. Lin–Vien.D, Colthup.N.B, Fateley.W.G, Grasselli.J.G, The Handbook of Infrared Raman Characteristic Frequencies of Organic Molecules, Academic Press, Boston, MA, 1991.
34. Surisseau.C, Marvell.P, J.RamanSpectro.25(1994) 447
35. Rogojerova.M, Kereszturyb.G, Jordanova.B, Spectrochim. Acta A 61 (2005) 1661-1670.
36. Hiremath. C.S, Yenagi.J , Tonannavar.J, Spectrochim. Acta A 68 (2007) 710-717
37. Arjunan.V, Saravanan.I, Ravindran.P, Mohan.S, Spectrochim. Acta A 74 (2009) 642-649.
38. V. Sortur, J. Yenagi, J. Tonannavar, V.B. Jadhav , M.V. Kulkarni , Spectrochim. Acta A 71 (2008) 688-694
39. Mahalakshmi.R.S, Vetrivelan.S, Irfan A, Muthu S. Absorption wavelength (TD-DFT) and adsorption of metal chalcogen clusters with methyl nicotinate: Structural, electronic, IRI, SERS, pharmacological and antiviral studies (HIV and omicron). Heliyon. 2023 May 13;9(5):e16066. https://doi.org/10.1016/j.heliyon.2023.e16066.
40. Bader.R.F.W, A quantum theory of molecular structure and its applications. Chem Rev 91(1991), 893–928.
41. Guillot.B, Viry.L, Guillot.R, Lecomte.C, Jelsch.C, Refinement of proteins at subatomic resolution with MOPRO. J Appl Crystallogr 34,(2001),214–223
42. Coppens.P, Abramov.Y, Carducci.M, Korjov.B, Novozhilova.I, Alhambra.C, Pressprich MR Experimental charge densities and intermolecular interactions: electrostatic and topological analysis of DL-histidine. J Am Chem Soc 121,(1999), 2585–2593

Figure 1: Theoretical optimized geometric structure with atom numbering of 4CBENC
Figure 2: The scan picture of 4CBENC
Figure 3: Correlation graph of heat capacity, entropy, enthalpy and temperature for 4CBENC
Figure 4: Dos graph UV graph of 4CBENC
Figure 5: Molecular orbitals and energies for the HOMO and LUMO of 4CBENC
Figure 6: Molecular electrostatic potential (MEP and ED) map in gas phase of 4CBENC
Figure 7: Experimental and simulated Infrared spectra of 4CBENC
Figure 8: Error analysis of wave numbers of 4CBENC
Figure 9: Analysis of Reduced density gradient (RDG) of 4CBENC
Figure 10: AIM of graph 4CBENC
Figure 11: Laplace diagram of the 4CBENC
Figure 12: Topological analysis of 4CBENC
Figure 13: Ramachandran Plot of 4CBENC

Table 1. Thermodynamic properties at different temperatures at the B3LYP/6-311++ G (d, p) level for 4CBENC			
T(K)	$C^0_{p,m}$ (cal mol^{-1} K^{-1})	S^0_m (cal mol^{-1} K^{-1})	ΔH^0_m (kcal mol^{-1})
100	17.507	78.670	1.338
200	31.063	94.980	6.207
300	45.950	112.530	11.328
400	60.154	129.397	16.655
500	74.119	145.586	21.017
600	80.230	158.351	30.517
700	86.035	170.779	39.872
800	93.137	184.537	49.638
900	99.351	197.002	58.515
1000	105.211	209.746	68.189

Table 2: Theoretical electronic absorption spectra of (absorption wavelength λ (nm), excitation energies E (eV) and oscillator strengths (f)) using TD-DFT/B3LYP/6-311++G(d,p) method in gas phase, Methanol and DMSO			
	λ (nm)	**E (eV)**	**(*f*)**
Gas	260.294	4.7621	0.0053
	253.757	4.8848	0.0015
	218.707	5.6691	0.0090
	214.481	5.7809	0.0080
	213.827	5.7979	0.0049
	207.743	5.9680	0.0007
	207.666	5.9684	0.9200
	204.832	6.0511	0.0269
	204.724	6.0541	0.0430
	195.934	6.3276	0.0002
Methanol	260.294	4.7632	0.0053
	253.757	4.8859	0.0015
	218.707	5.6689	0.0090
	214.481	5.7806	0.0080
	213.827	5.7806	0.0049
	207.743	5.9681	0.0007
	207.666	5.9703	0.9200
	204.832	6.0529	0.0269
	204.724	6.0561	0.0430
	195.934	6.3278	0.0002
DMSO	260.119	4.7664	0.0061
	253.565	4.8896	0.0014
	219.408	5.6508	0.0153

	215.286	5.7590	0.0091
	214.307	5.7853	0.0078
	208.214	5.9546	0.9554
	208.011	5.9604	0.0009
	204.799	6.0539	0.0239
	204.576	6.0605	0.0456
	192.076	6.4549	0.0001

Table 3: Experimental (FT-IR) wavenumbers and detailed assignments of theoretical wavenumbers of along with potential energy distribution.

Sl.No	S^y	FTIR	Scaled				Vibrational assignment With PED
			I^{IR}	I^{Ra}	HF	B3LYP	
1.	A′		0.09	33.87	3076	3082	γCH(98)
2.	A′		0.17	14.07	3063	3069	γCH(100)
3.	A′		0.30	44.45	3046	3051	γCH(95)
4.	A′	3050 vw	4.28	4.66	3045	3052	γCH(92)
5.	A′		24.49	34.44	3025	3031	γCH(96)
6.	A′		15.27	46.41	3025	3030	γCH(92)
7.	A′	3020 vw	2.35	77.96	3010	3016	γCH(98)
8.	A′		7.51	42.76	3008	3015	γCH(97)
9.	A′		8.12	77.54	2987	2993	γCH(98)
10.	A′	1575 vw	2.71	244.23	1495	1569	γCC(82)
11.	A′	1550 vw	31.58	83.74	1481	1555	γCC(74)
12.	A′		67.44	24.62	1480	1538	γCC(70)
13.	A′		14.97	1.40	1478	1535	γCC(78)
14.	A′	1475 vs	31.23	20.43	1453	1462	γCC(71)
15.	A′	1450 m	26.89	46.77	1440	1457	γCC(73)
16.	A′		16.27	0.63	1434	1427	γCC(69)
17.	A′	1410 m	22.26	2.58	1353	1410	γCC(71)
18.	A′		1.32	46.64	1326	1377	γCC(66)
19.	A′		0.12	4.62	1296	1309	γCC(81)
20.	A′	1310 vw	0.24	45.45	1281	1308	γCC(80)
21.	A′	1275 vw	1.92	67.64	1231	1276	γCC(75)
22.	A′		6.56	5.77	1228	1254	γCC(68)
23.	A′	1190 vw	0.61	2.83	1169	1199	βCH(58)
24.	A′	1175 vw	24.80	83.02	1153	1184	βCH(61)
25.	A′		0.97	24.12	1123	1158	βCH(55)
26.	A′	1150 vw	0.58	7.30	1120	1152	βCH(62)
27.	A′	1095 vs	6.10	0.34	1060	1092	βCH(68)
28.	A′		6.58	3.04	1052	1083	βCH(58)
29.	A′		41.69	42.58	1027	1069	βCH(68)

30.	A′	1055 vw	5.26	2.90	1025	1064	βCH(63)
31.	A′		10.18	08.10	947	969	βCH(61)
32.	A′		6.43	7.42	934	964	γCCC(64)
33.	A′	950 vw	0.34	0.12	913	945	γCCC(66)
34.	A′		0.04	3.16	912	945	γCCC(69)
35.	A′	915 vw	16.56	1.33	866	910	γCCC(55)
36.	A′		0.62	8.67	848	889	γCCC(58)
37.	A′		30.58	1.06	843	873	γCCC(49)
38.	A′		6.44	1.37	834	870	γCCC(62)
39.	A′		18.84	7.85	829	859	γCCC(49)
40.	A′	850 m	19.69	1.66	817	852	γCCC(53)
41.	A′		50.79	3.44	743	778	γCCC(57)
42.	A″	760 m	0.52	5.10	729	762	φCH(51)
43.	A″	720 vw	11.34	0.43	697	723	φCH(55)
44.	A″	695 s	18.44	1.73	669	687	φCH(48)
45.	A″		21.59	6.74	654	678	φCH(45)
46.	A″	668 vw	12.43	7.94	629	663	φCH(49)
47.	A″		22.44	1.99	612	656	φCH(41)
48.	A″	610 s	0.50	5.83	605	627	φCH(39)
49.	A″		8.76	2.12	550	563	φCH(48)
50.	A″		0.06	1.66	499	530	φCH(49)
51.	A″	515 vw	0.59	2.64	498	527	φCCC(45)
52.	A″		0.19	0.24	405	434	φCCC(46)
53.	A″	430 vw	4.67	0.83	405	433	φCCC(44)
54.	A′	405 vw	1.17	1.20	398	403	γCCl(59)
55.	A′		7.36	12.17	393	397	γCCl(61)
56.	A″		0.43	0.57	357	359	φCCC(49)
57.	A″		0.03	1.01	304	308	φCCC(45)
58.	A′		0.00	2.39	275	284	βCCl(54)
59.	A′		0.55	4.35	254	268	βCCl(51)
60.	A″		0.01	4.83	186	197	φCCC(40)
61.	A″		0.06	5.96	172	181	φCCC(38)
62.	A″		0.12	4.23	171	180	φCCl(45)
63.	A″		0.32	3.29	152	156	φCCl(49)
64.	A″		0.32	1.97	54	55	φCCC(39)
65.	A″		0.00	2.87	52	54	φCCC(36)
66.	A″		0.05	9.20	30	31	φCCC(38)

s: strong; vs: very strong; m: medium; w: weak; vw: very weak. [b] γ: stretching; β: in-plane bending; φ: out-of-plane bending; I^{IR}: Infrared intensity; S^{a}: Raman activity; S^{y}: Symmetry species

Table 4. AIM analysis of the some Bond Critical points (BCP) of 4CBENC at B3LYP/6-311++G(d,p) level					
Parameter (a.u.)	$\rho(r_c)$	$\nabla^2\rho(r_c)$	λ_1	λ_2	λ_3
RC1	0.0211	-0.0322	-0.0113	0.0653	0.0749
RC2	0.0097	-0.0095	-0.0022	0.0092	0.0309
RC3	0.0211	-0.0322	-0.0113	0.0653	0.0749
RB1	0.28153	0.2019	-0.5368	-0.4732	0.2021
RB2	0.2796	0.1994	-0.5303	-0.4666	0.1990
RB3	0.3033	0.2199	-0.5919	-0.4992	0.2112
RB4	0.2980	0.2147	-0.5783	-0.4959	0.2151
RB11	0.2725	0.1928	-0.5151	-0.4622	0.2059
RB15	0.2796	0.1994	-0.5303	-0.4666	0.1990
RB14	0.0114	-0.0109	-0.0077	-0.0049	0.0565
RB26	0.1444	0.0237	-0.1934	-0.1876	0.2859
RB25	0.1444	0.0237	-0.1934	-0.1876	0.2859
RB20	0.2431	0.0701	-0.4508	-0.3851	0.5552
RC1: Unit 1; RB1: Unit 2 formed					

Table 5. Idealized φ and ψ angles for common secondary structures in proteins		
Secondary structure	Torsion angles (degrees)	
	φ	ψ
Antiparallel β-sheet	-50 to -150	100 to 170
Parallel β-sheet	-75 to -135	70 to 135
Collagen	-70 to -100	25 to 45
Left-handed α-helix	25 to 65	45 to 90
Right-handed α-helix	-10 to -75	-60 to -130